ACTA MECHANICA SINICA, Vol.11, No.3, August 1995 ISSN 0567-7718
The Chinese Society of Theoretical and Applied Mechanics
Chinese Journal of Mechanics Press, Beijing, China
Allerton Press, INC., New York, U.S.A.

ON LASER-INDUCED REVERSE PLUGGING EFFECT*

Duan Zhuping (段祝平) Zhou Yichun (周益春) Huang Chengguan (黄成光)
(LNM and Laboratory for Laser and Dynamic Behaviors of Materials
Institute of Mechanics, CAS, Beijing, 100080, *China)*

ABSTRACT: A new kind of failure induced by long pulsed laser, named as reverse plugging effect (RPE), was experimentally observed in thin foil of brass. The whole failure process can be divided into three stages, namely thermal reverse bulging, shear deformation localization and reverse perforation. In this paper, a description of experimental and theoretical study on this newly discovered phenomenon is presented in detail.

KEY WORDS: reverse plugging effect, laser-material interaction, shear deformation localization, dynamic failure, long pulsed laser

I. INTRODUCTION

Interaction of laser with materials leads, in general, to two kinds of coupled damage, mechanical and thermal damage, depending on laser parameters and target material thermal mechanical properties. Laser induced damage has been extensively studied during the past two decades[1−4]. However, in previous studies on laser-induced damage people more and less ignored the fact that the temporal and spatial shapes of the laser beam intensity could also play an important role in controlling the damage pattern. In other words,even if the average intensity and duration of the laser remain the same, material damage can also be altered by changing the spatial and temporal characteristics of the laser beam. Our experimental research offers a proof of this statement. During the past two years when the authors have studied the interaction of long-pulsed Nd:Glass laser with a thin plate of brass, and found through experiments a new type of laser induced damage,which they now term the reverse plugging effect (RPE). The whole process of laser induced reverse plugging consists generally of three stages,i.e.,reverse thermal bulging, shear deformation concentration and localization, and plugging-like fracture. This particular type of failure induced by laser is similar to the general plugging (GPE), which happens when a thin plate is penetrated normally by a rigid projectile. The difference between the two types of plugging is in the plugging direction. In the GPE case, plugging is in the direction of the moving projectile, while, in the RPE case, plugging is opposite to the incident laser beam direction. Motivated by this comparison, the authors called this particular failure mode the reverse plugging effect, which, to the best of their knowledge, has not been reported in the literature.

Received 27 December 1994
Concurrently published in the Chinese Edition of Acta Mechanica Sinica, Vol.27, No.3, 1995
* The project supported by the National Natural Science Foundation of China and the Field of Laser Technology, 863-NHT Research Development Program

This paper presents a detailed description and analysis of this newly-discovered phenomenon. Following this introductory section, the experimental method for the RPE is described in section II, where the result of the microscopic examination of damage by SEM on the tested and sectioned samples is presented. In section III, an analytical solution for 2-D axial-symmetrical temperature fields is given by means of Hankel transformation and series expansion techniques. Using this temperature solution and classical Kirchhoff plate theory, the deflection curve,i.e.,the thermal reverse bulging can be determined analytically under the assumption of thermal-mechanical decoupling. In section IV, a simple axial-symmetrical shearing model is proposed using the Bodner-Partom constitutive law[5] to examine the shear stress and shear strain concentration within the LSE-region, i.e.,the laser spot edge region. A modified finite element method (MFEM) and a corresponding computational code are developed for the numerical simulation of this complicated problem.

II. EXPERIMENTAL METHOD AND OBSERVATIONS

The experimental study of RPE was performed using a multi-mode, single pulsed Nd:Glass laser with wavelength $\lambda = 1.06\mu$m and maximum energy up to 300J. The optical path and device arrangement are schematically shown in Fig.1.

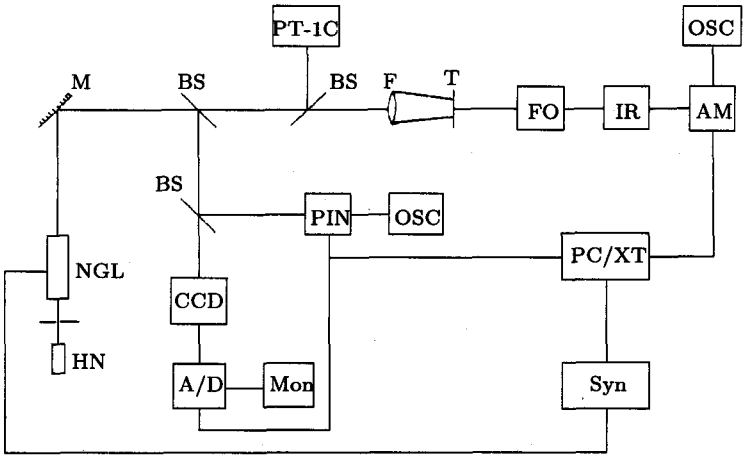

Fig.1 Optical path and device arrangement in the test.
NGL=Nd:Glass laser, HN=He-Ne laser, M=Mirror, BS=beamsplitter, CCD=charge-coupled device sensor, A/D=A/D transformer, Mon=Monitor, PIN=PIN photoelectric cell, OSC=oscillograph, PT-1C=PT-1C laser energy recorder, F=focalizer(f=100mm), T=target, FO=focusing optics, IR=InSb infrared detectors, Am=amplifier, PC/XT=PC/XT personal computer, Syn=synchronizer

The diagnostics of the laser parameters provide a traditional monitoring of the laser beam characteristics, such as total energy, temporal and spatial shapes, light spot size,etc. A PIN photoelectric cell with the corresponding response time less than 1.0ns was used to directly measure the temporal shape of laser intensity and its spatial shape was detected by a CCD sensor. These shapes are shown in Fig.2 and Fig.3, respectively.From these measurements, it is seen that the laser intensity rises rapidly within 50μs, and then decays exponentially with a sawtooth-like oscillation. The full width at half maximum (FWHM) of the laser is approximately 250μs. We should mention that the IR sensor to measure the

temperature rise on the rear surface has not been used yet in the test. The typical spatial profile is non-Gaussian form and roughly uniform within the laser irradiated region, and declines very sharply in the LSE-region. For the convenience of numerical analysis, the laser intensity I is approximated by

$$I = I_{\max} e^{-\alpha t}(1 - e^{-\beta t}) f(r) = I_{\max} g(t) f(r) \tag{2.1}$$

where α and β are determined experimentally, and are equal to 1.5×10^{-4}/s and 8×10^{-4}/s, respectively. Therefore, laser energy $E_J = \beta\pi a^2 I_{\max}/\alpha(\alpha+\beta)$ and we have

$$f(r) = \begin{cases} 1 & 0 \le r < a \\ 0 & a \le r < \infty \end{cases} \tag{2.2}$$

to account for the non-Gaussian nature of the laser beam, where r is the radial coordinate and a laser spot radius. In the following, the region $0.95a \le r \le 1.05a$ is called the laser spot edge region and is labelled as the LSE-region for convenience.

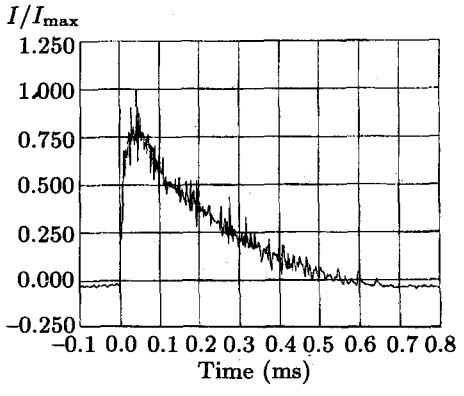

Fig.2 Temporal shape of Nd:Glass pulsed laser

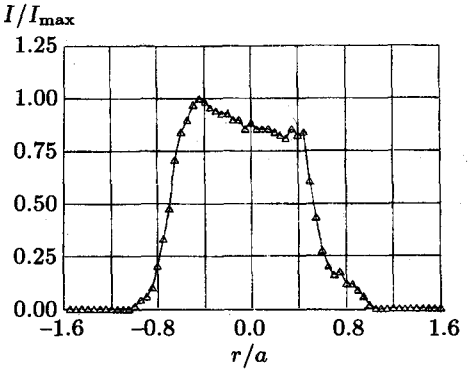

Fig.3 Laser pulse spatial configuration

The target material is brass, which is composed of 65.5% copper (in weight), 33.6% zinc, 0.03% iron, 0.06% amtimony as well as extremely small amount of several other elements. The samples are circular in shape with 30mm in diameter and 0.1mm in thickness, and they are clamped by a big circular holder on its edge during the test. The laser energy used in the test ranges from 25~40J and therefore, its intensity is on the order of $10^5 \sim 10^6 \mathrm{w/cm}^2$.After the test, each sample is examined using a conventional optical microscopy. A typical micrograph is shown in Fig.4. This picture clearly shows thermal reverse bulging of the laser irradiated region and plastic shear deformation localized in the LSE-region.The maximum deflection at the center of the plate is 0.03mm. In order to further examine the damage in the LSE-region, metallurgical or scanning electron microscopy (SEM) is employed. The SEM-micrograph for the shear deformation localization in the LSE-region is seen in Fig.5 and Fig.6. From the SEM observation, one infers that the thermal stress-induced microcrack initiates on the rear surface within the LSE-region and then propagates axially. Growth and coalesence of such microcracks will lead to the formation of a circular macrocrack through the target thickness.A shear fractograph viewed from the rear surface is shown in Fig.6. One can see from this figure that the fractograph looks like landslide, i.e., the profile of the snake−like pattern. This is a typical plugging−type fractograph. In addition, a comparison was made of the SEM taken from both the GPE and the RPE samples. This comparison of the micrographs (in Fig.7(a)–(b)) displays the close similarity in failure characteristics.

Additionally, experimental results from the macroscopic measurement are given in Table 1. When the laser energy density is lower than 150J/cm^2,or equivalently the laser intensity is less than $0.51\times10^6\text{w/cm}^2$,no evident damage can be observed macroscopically on the front and rear surfaces of the samples. The intensity threshold I_{cr} for initiating RPE is about $0.61\times10^6\text{w/cm}^2$. As I exceeds the value I_{cr},a few melted spots can be observed in the LSE-region on the front surface of the sample. As long as the laser intensity equals or goes beyond the value of $0.75\times10^6\text{w/cm}^2$, the metallic sheet is entirely fractured and fragmented.In this case, part of material within the LSE-region is found melted apparently. The whole process of the reverse plugging is schematically shown in Fig.8.

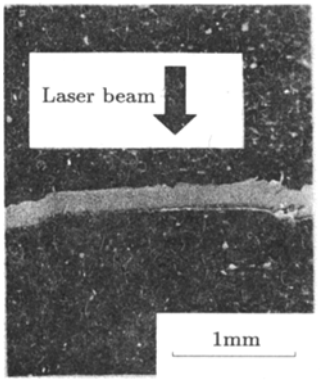

Fig.4

Fig.5

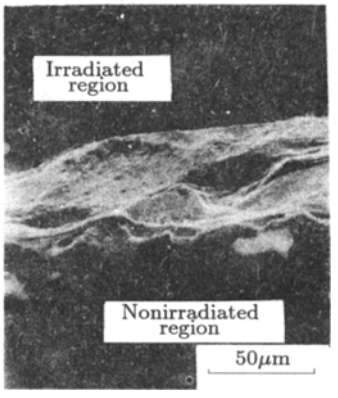

Fig.6

Fig.4 Reverse bulging and shear deformation concentration in the LSE-region (viewed laterally, $E_j = 8.2\text{J}, 2a = 2.3\text{mm}$)

Fig.5 Micro-crack initiates first on the rear surface within the LSE-region and then propagates axially

Fig.6 Shear fractograph is viewed from the rear surfaces ($2a = 4.5\text{mm}, E_J = 31\text{J}$)

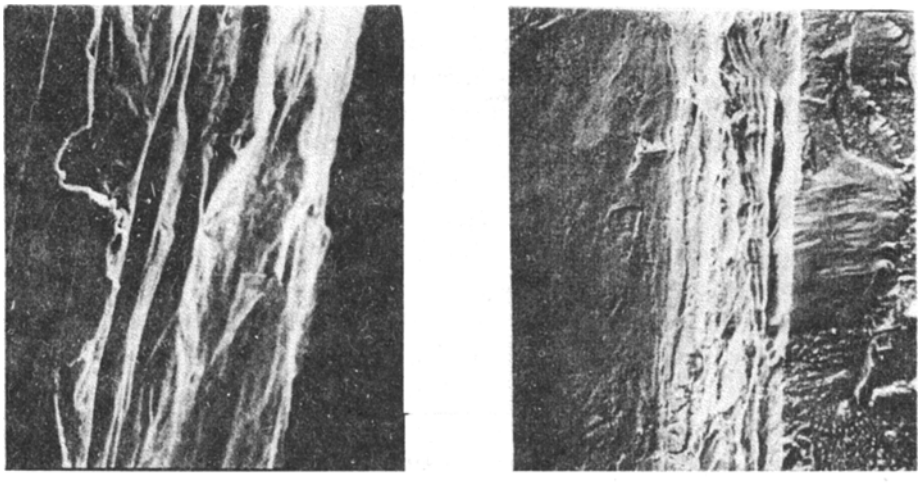

(a) (b)

Fig.7 Direct observation and comparison for the fractographs taken either from laser irradiated sample (a) and from mechannical loaded sample (b)

Table 1

Macro-Phenomena and Energy Threshold to Produce Damage

No.	Energy $E_J(J)$	Laser spot diameter (mm)	Energy density (J/cm^2)	Intensity (MW/cm^2)	Spall threshold (J/cm^2) ($\tau = 4.0ns$)	Macro-phenomena
1	29.6	5.0	151	0.51	210	(1)
2	33.2	5.0	169	0.56	210	(2)
3	35.7	5.0	182	0.61	210	(3)
4	38.3	5.0	195	0.65	210	(4)
5	41.6	5.0	213	0.71	210	(5)
6	44.1	5.0	226	0.75	210	(6)

(1) No observable macor-damage
(2) In LSE-region, little melted material is observed on the front surface of the thin plate. The irradiated region bulges in the opposite direction of the incident laser.
(3) In LSE-region, there is a little of melted materials on the irradiated surface and the RPE on the rear surface can be visualized.
(4) The phenomena are the same as the above.
(5) The laser irradiated part just separated from its edge.
(6) Fragmented completely.

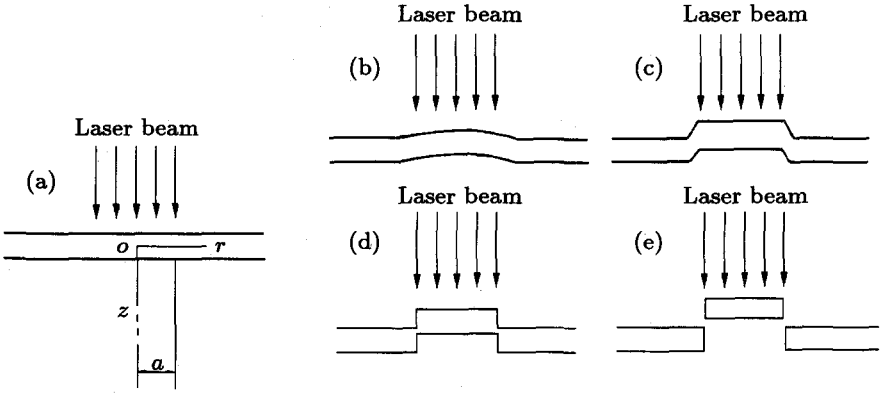

Fig.8 Three stages of laser induced deformation and failure: thermo-elastic bulging (b), shear deformation localization and fracture ((c) and (d)) and fragmentation (e)

III. TEMPERATURE FIELDS AND THERMAL ELASTIC REVERSE BULGING

Determination of the temperature rise $\theta = T - T_0 = \theta(r, z, t)$ is essential in finding its dependence on laser parameters and in revealing the mechanism for RPE,where T and T_0 are the absolute temperature and room temperature, respectively. To arrive at this goal, we assume:

(1) The laser is the only source of heat supply to the target material and the contribution to temperature rise through mechanical work is neglected.
(2) There is no solid to liquid phase transformation during laser irradiation.
(3) The deformation is infinitesimal and axial-symmetric so that the calculation can be based on the initial configuration.

(4) All thermal and mechanical material parameters are independent of temperature.

(5) The thermal irradiation from both surfaces of the sample is negligible in comparison with the laser energy absorbed.

Clearly, under these five assumptions, the temperature field satisfies 2-D heat diffusion equation:

$$\frac{\partial \theta}{\partial t} = D\Big(\frac{\partial^2 \theta}{\partial r^2} + \frac{1}{r}\frac{\partial \theta}{\partial r} + \frac{\partial^2 \theta}{\partial z^2}\Big) \tag{3.1}$$

with initial and boundary conditions

$$\theta\Big|_{t=0} = 0 \tag{3.2}$$

$$\left.\begin{aligned} &\frac{\partial \theta}{\partial r}\Big|_{r=0} = \theta\Big|_{r=b} = 0 \\ &\frac{\partial \theta}{\partial z}\Big|_{z=\frac{h}{2}} = 0 \qquad \frac{\partial \theta}{\partial z}\Big|_{z=-\frac{h}{2}} = -\frac{1}{\kappa}(1-R_0)I_{\max} f(r)g(t) \end{aligned}\right\} \tag{3.3}$$

where the condition $(3.3)_3$ represents the laser absorption by the front surface $z = -h/2$ of the target material, in which h is the target thickness, b is the outer radius of the sample and is taken larger enough as compared to the laser spot size a, $D = \kappa/\rho C_p$ is thermal diffusion coefficient, κ thermal conductivity, C_p heat capacity ,R_0 the reflection coefficient and the laser intensity $I_{\max}$ is given in (2.1).

Using Hankel transformation and Bessel series expansion technique, the problem (3.1)–(3.3) was solved analytically by Zhou et al.[6]. This solution is given in a non-dimensional series expansion form, which mainly depends on the following four dimensionless parameters

$$A = \frac{\alpha a^2}{D} \qquad B = \frac{(\alpha+\beta)a^2}{D} = A(1+\frac{\alpha}{\beta}) \qquad h_1 = \frac{h}{a} \qquad h_4 = \frac{(1-R_0)I_{\max}a}{\kappa T_m} \tag{3.4}$$

where $h_2 = b/a$, and $A, B, h_1, h_2, h_4, D, R_0$ are 2800, 1.77×10^4, 0.04, 1.4, 58.7, $0.335\text{cm}^2/\text{s}$, 0.90, respectively.

Some calculated results for the temperature θ are depicted graphically in Figs.9(a)–(b). From these pictures, one can see that (a) the temperature gradient in z-direction, i.e., $\dfrac{\partial \theta}{\partial z}$ is high in the early stage of laser irradiation. This is a key factor in producing thermal bulging; (b) the spatial profile of temperature field is influenced definitely by the spatial shape of laser beam, therefore, Gaussian and non-Gaussian types of laser beam lead to different temperature field even though the net energy and duration are the same.For the non-Gaussian type laser used in this work, a sharp drop in temperature takes place inside the LSE-region.

Now, let us move on to the computation of transverse deflection. Suppose the membrane and shear forces can be neglected, and classical Kirchhoff plate theory can be used for the deflection $w = w(r,t)$, then we have

$$D_1\Delta^2 w + \frac{1}{1-\nu}\Delta M_t + \rho h\ddot{w} = 0 \tag{3.5}$$

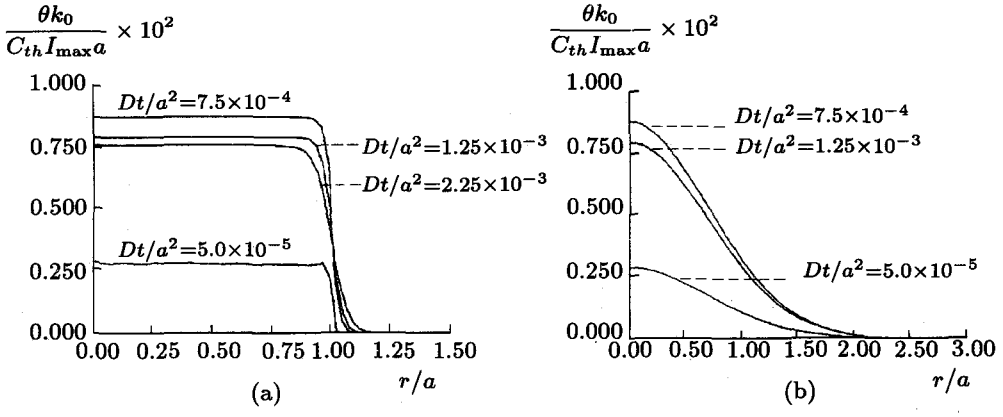

Fig.9 Variations of nondimensional temperature rises with r/a on the front surface at different time, where the spatial shape of laser beam is non-Gaussian (a) or Gaussian (b) type

with the initial and boundary conditions

$$\left.\begin{aligned} & w\big|_{t=0} = \frac{\partial w}{\partial t}\Big|_{t=0} = 0 \\ & w\big|_{r=0} = \frac{\partial w}{\partial r}\Big|_{r=0} = \text{finite} \qquad w|_{r=b} = \frac{\partial w}{\partial r}\Big|_{r=b} = 0 \end{aligned}\right\} \qquad (3.6),(3.7)$$

respectively, where Δ is the Laplace operator given in axial-symmetrical coordinate system, $D_1 = \dfrac{Eh^3}{12(1-\nu^2)}$ denotes the bending stiffiness, where E and ν are, respectively, Young's modulus and Poisson ratio, ρ the mass density. In (3.5), M_t is the equivalent thermal bending moment given by

$$M_t = \alpha_0 E \int_{-h/2}^{h/2} \theta(r,z,t) z \mathrm{d}z \qquad q_\theta \equiv -\frac{1}{1-\nu}\Delta M_t \qquad (3.8)$$

where α_0 is the thermal expansion coefficient. Since the temperature $\theta = \theta(r,z,t)$ has already been obtained from the solution[6] of Eqs.(3.1)–(3.3), the thermal moment M_t and the equivalent transverse loading q_θ can be completely determined before solving (3.5) for w. Numerical results for q_θ are schematically shown in Fig.10(a)–(b) in the cases of Gaussian and non-Gaussian types of beam. The difference between the two cases is evident.

To solve Eq.(3.5) with the conditions (3.6)–(3.7), we decompose w into two parts[15]: the quasi-static part w_s and dynamic part w_d

$$w = w_s + w_d \qquad (3.9)$$

These solutions w_s and w_d are obtained using a series expansion technique[8]. Typical results of the deflections for w, w_s and w_d are respectively depicted in Fig.11. These results again confirm that the target sheet subjected to laser heating does bulge in the opposite direction towards laser incidence. The temperature profiles and equivalent transverse thermal loading q_θ vary with r in the LSE-region much more rapidly in the non-Gaussian case than in the case of Gaussian type of laser.So does the curvature of the deflection curves. On the other hand, since the equivalent thermal stress in the LSE-region has already exceeded

the corresponding yield stress under the elevated temperature condition, developing a thermal elasto-plastic coupling theory for the study of thermal shear stress concentration in the LSE-region plays actually an essential role in understanding of RPE at the second stage of laser irradiation.

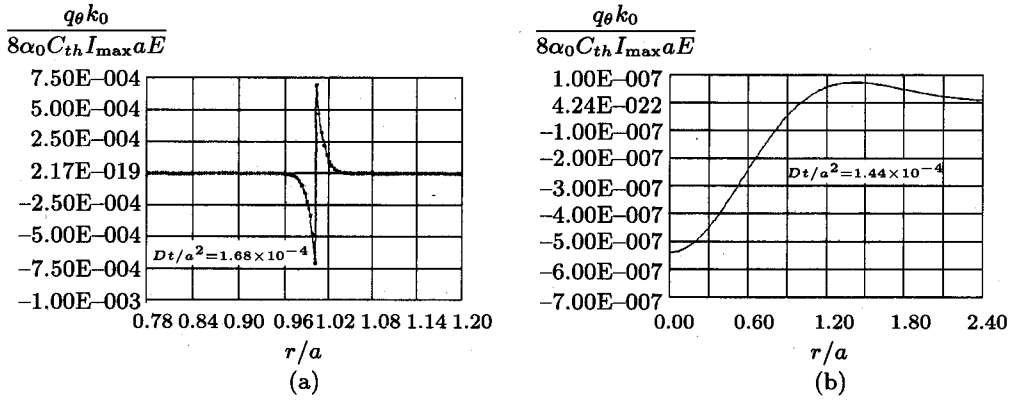

Fig.10 Spatial distribution of equivalent external loading induced by either square-typed (a) or Gaussian laser beam (b), where $M_p = 8\alpha_0 T_m h_4 E/\sigma_0^0$ and σ_0^0 yield strength at room temperature

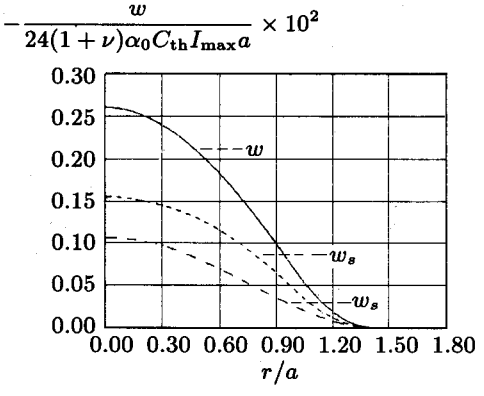

Fig.11 Deflection curve calculated for the thin plate, where $W_p = 24(1+\nu)\alpha_0 T_m h_4$ and $D_t/a^2 = 3.0 \times 10^{-4}$

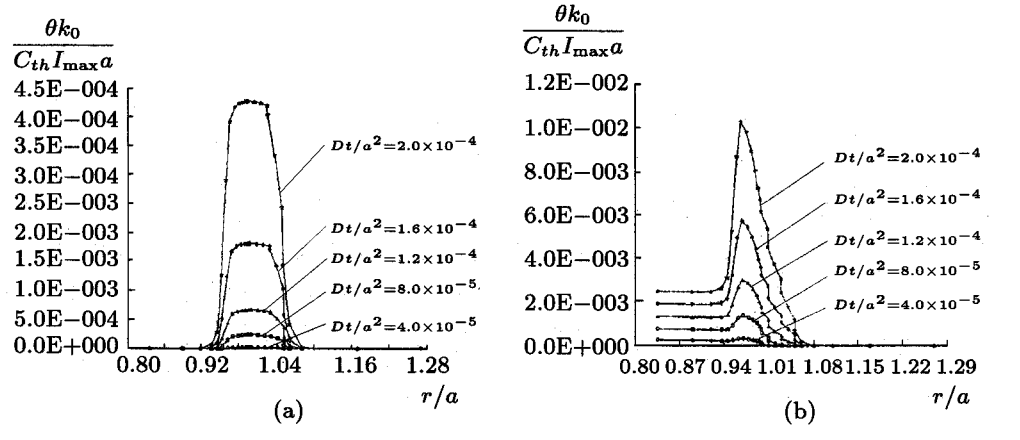

Fig.12 Variations of temperature with r/a at different time

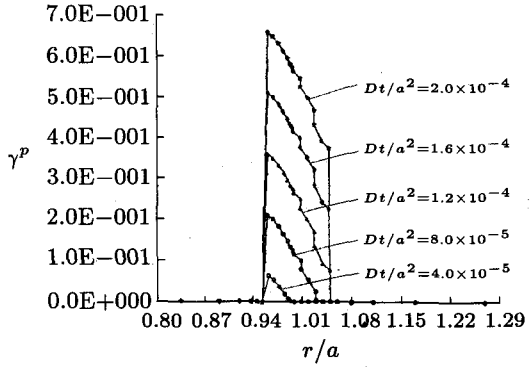

Fig.13 Variations of plastic strain with r/a at different time

IV. A SIMPLE AXIAL-SYMMETRIC SHEAR MODEL FOR ANALYSIS OF DEFORMATION CONCENTRATION

In this section, a simple elastic visco-plastic shear model is proposed in cylindrical coordinate system for the analysis of thermal shear force concentration in the LSE-region. During the whole process of laser irradiation, only a small portion of the absorbed laser energy by the target can be transformed into its kinetic energy, contributing to the reverse motion for the laser irradiated inner region $0\leq r\leq 0.95a$. This kinetic energy will promote the shear deformation concentration in the LSE-region. To explore the physical mechanism controlling the shear deformation concentration and the thermal-mechanical coupling phenomenon in the LSE-region, it is assumed that

(1) The shear stress τ_{rz} or the average shear force $\hat{\tau}$ dominates the failure process of reverse plugging in the LSE-region in comparison with the stress components σ_r and σ_θ.

(2) The target material within the laser irradiation region $0\leq r\leq 0.95a$ moves as a rigid body towards the opposite direction of laser incidence with a time-dependent velocity $v_0 = v_0(t)$, which can be globally and solely determined by the kinetic energy transformed from a small portion of total laser energy absorbed by the target.

(3) The material obeys the thermal elastic visco-plastic constitutive law suggested by Bodner and Partom[5].

Under the above assumptions, the governing equations in the shear zone for the axial symmetric simple shear model can be obtained as

$$\frac{1}{r}(r\hat{\tau})_{,r} = \rho\dot{v} \qquad \hat{\tau} \equiv \frac{1}{h}\int_{-h/2}^{h/2}\tau_{rz}\mathrm{d}z \tag{4.1}$$

$$\rho C_p\dot{\theta} = \frac{1}{r}[r\kappa\theta_{,r}]_{,r} + \eta\dot{W}_p + q_l \tag{4.2}$$

$$v_{,r} = \frac{1}{\mu(T)}(\dot{\hat{\tau}}) + \dot{\gamma}^p \tag{4.3}$$

$$\dot{\gamma}^p = D_0\exp\Big\{-\frac{1}{2}\Big[\frac{\hat{Z}}{\sqrt{3}\hat{\tau}}\Big]^{2n(T)}\Big\} \tag{4.4}$$

$$\hat{Z} = Z_1 - (Z_1 - Z_0)\exp(-mW_p) \tag{4.5}$$

$$\dot{W}_p = \hat{\tau}\dot{\gamma}^p \tag{4.6}$$

$$q_l(r,t) = (1-R_0)I_{\max}g(t)f(r)/h \tag{4.7}$$

where $\hat{\tau}, v$ and θ represent, respectively, the average shear force, particle transverse velocity and instantaneous temperature, W_p is the plastic deformation work, of which most part ($> 85\%$) η is dissipated as heat as pointed out by Taylor and Quinney[9], the temperature-dependent shear modulus $\mu(T)$ and $n(T)$ are assumed to take the form

$$\mu(T) = \mu_0\Big\{1 - \frac{T-T_0}{T_m-T_0}\exp\Big[-\xi\Big(1-\frac{T-T_0}{T_m-T_0}\Big)\Big]\Big\} \quad n(T) = \frac{T_m}{T} \tag{4.8}$$

where μ_0 is the shear modulus under room temperature, T_m the melting temperature, T_0 room temperature. In Eqs.(4.5) and (4.8), D_0, Z_1, Z_0, m and ξ are the material parameters as given in Table 2.

Table 2
Material Parameters

ρ(g/cm^2)	C_p(J/g.K)	κ(w/cm.K)	μ_0(GPa)	T_0(K)	$D_0(s^{-1})$
8.7	0.37	1.09	43.0	300	2.0×10^4
T_m(K)	ξ	Z_0(GPa)	Z_1(GPa)	m(GPa)$^{-1}$	η
1356	4.23	0.68	0.87	87.0	1.0

To solve the system of Eqs.(4.1)−(4.6), the initial and boundary conditions as well as symmetric condition for $\hat{\tau}, \theta$ and v are formulated as

$$v\Big|_{t=0} = \theta|_{t=0} = \hat{\tau}|_{t=0} = 0 \tag{4.9}$$

$$v\Big|_{r\geq 1.05a} = \theta_{,r}|_{r=0} = \theta_{,r}|_{r=b} = 0 \tag{4.10}$$

$$v\Big|_{r\leq 0.95a} = -\Big[2\frac{\eta_0 I_{\max}(1-R_0)}{\rho h}g(t)\int_0^t g(\tau)\mathrm{d}\tau\Big]^{1/2} \tag{4.11}$$

where the last condition (4.10) shows that only a small portion of the total absorbed laser energy, saying η_0, by target is converted into the kinetric energy of the material within the irradiated region. Based on the calculated results given in section III of thermo-elastic bulging analysis, we take $\eta_0 = 0.001$.

In seeking the solution of the thermal-mechanical coupling system (4.1)−(4.6), a modified finite element method 1-D code was developed based on the stress compatible iteration technique proposed by Song[10]. The conventional finite element method is modified in such a way that the continuity and compatibility conditions in velocity and stress from one element to the neighboring ones must be ensured by introducing a nonlinear interpolution function in FEM computational code.

Some numerical results gained by means of this modified finite element technique are depicted in Figs.12 and 13, illustrating the variations of v, θ and γ^p with r at different time during reverse plugging . For instance, one can see from Fig.13 that the temperature rises in LSE-region much faster than within the inner laser spot region. The highest temperature in this narrow region reaches at $r = 0.97a$ and is close to the melting temperature of the material. This temperature characteristics appears exceptionally different from that obtained by thermo-elastic plate decoupling theory as descrived in detail in section II. This

temperature rise is contributed not only by laser irradiation but also by heat conduction as well as the dissipation of plastic deformation energy. A comparison is also made in Fig.14 to show each contribution to temperature rise from these three events. As one can see in the early period of laser irradiation, the laser energy supply plays a dominating role in leading to the increase in temperature. However, this role decreases exponentially with time. Instead, in the later stage of laser irradiation, heat conduction and dissipation of plastic energy become main factors controlling the temperature rise and concentration in this region, where the thermo-plastic strain γ^p is sharply accumulated as seen from Fig.13, i.e., the plastic shear strain γ^p increases very steeply near $r = 0.95a$, then linearly decreases with r, and tends to zero at $r = 1.05a$. The numerical procedure can be simplified naturally to the so-called conventional plugging problem by deleting the external heat source term q_l in Eq.(4.2) and letting the velocity $v|_{r\leq 0.95a}$ be constant. However, in this case, θ and γ^p are distributed in a quite different manner from the former case. The comparision for the both cases is also illustrated in the Fig.14. From this comparision, one concludes that the thermal-mechanical coupling dominates the reverse plugging process in the shear zone in the later stage of laser irradiation and should not be ignored in computation.

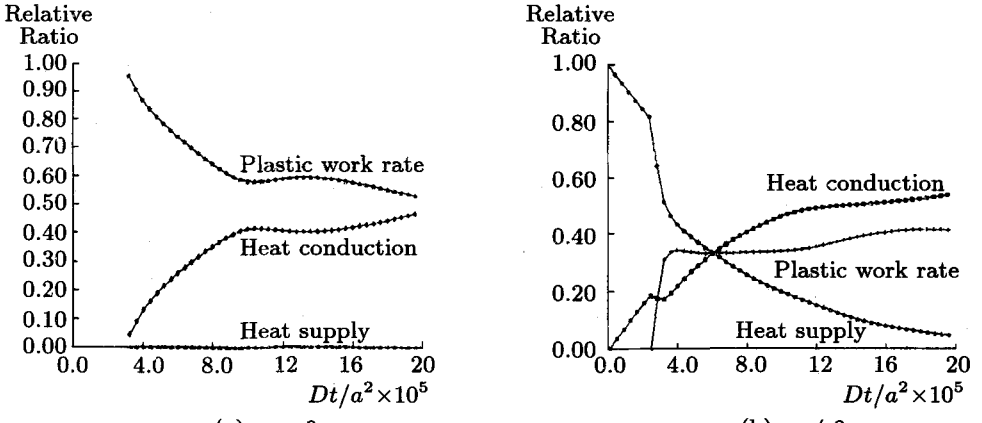

Fig.14 Comparison of contributions due to heat conduction, plastic work rate, laser heat supply to the temperature rise in the LSE-region

V. CONCLUSION AND FUTURE WORK

A new kind of laser-induced failure mode, namely the reverse plugging effect has been first reported experimentally. In order to theoretically explain this newly-discovered phenomenon, two different simple models were suggested. Using a classical thermal-elastic decoupling plate theory, an analytical solution for temperature field and transverse deflection for the thin plate of brass are obtained. The thermal-mechanical coupling theory is utilized to analyze the non-adiabatic thermal plastic deformation on the margin area of laser spot. The second model in connection with numerical results could provide us at least semi-quantitatively a mechanical basis to explain reasonably the faster temperature rise with subsequent material thermo-softening. Clearly, when the laser intensity I is below some critical value I_{cr} so that the target material within the LSE-region is not melted, it is this temperature rise and subsequent deformation localization that control the whole pro-

cess of reverse plugging. Since this failure process involves many multi−interrelated physical mechanisms, much work is left for further investigation, including: (a) a more reasonable constitutive law, damage evolution and failure criterion used for the theoretical and numerical analysis; (b) scalling law for RPE; (c) development of 2-D FEM dynamic code for a more sophisticated numerical simulation, including the shear stress concentration induced failure phenomenon;(d) an elaborate experimental measurements for the instantaneous temperature and strain distributions, particularly in the LSE-region. All the mentioned work is now being under investigation in our laboratory.

Acknowledgement Authors would like to express their sincere thanks to Profs. Zheng Zhemin and Xie Bomin for their valuable discussions given during the preparation of this paper.

REFERENCES

[1] Ready JF. Effects of high-power laser radiation. Academic Press. 1971
[2] von Allmen M. Laser-beam interactions with materials. Springer-Verlag. 1987
[3] Kar A, Mazumder J. *J Appl Phys*, 1990, 68(8): 3884–3891
[4] Eliezer S, Gilath I, Bar-Noy T. *J Appl Phys*, 1990, 67(2): 715–724
[5] Bodner SR and Partom Y. *J Appl Mech*, 1975, 42(2): 385–389
[6] Zhou YC. Experimental and theoretical studies on long pulsed laser induced reverse plugging effect, PhD Thesis. Insitute of Mechanics, Chinese Academy of Sciences, 1994
[7] Tauchert TR. *J Thermal Stress*, 1989, 12(3): 241–258
[8] Zhou YC, Duan ZP, Xie BM. Submitted to Applied Mathematics and Mechanics for publication (in Chinese)
[9] Taylor GI, Quinney H. Proc R Soc, 1934, A143: 307–326
[10] Song SC. *Applied Mathematics and Mechanics*, 1989, 10 (2): 137–143 (in Chinese)